Conducting wall Hall thrusters in magnetic shielding and standard configurations

Lou Grimaud and Stéphane Mazouffre

Citation: Journal of Applied Physics **122**, 033305 (2017); doi: 10.1063/1.4995285
View online: http://dx.doi.org/10.1063/1.4995285
View Table of Contents: http://aip.scitation.org/toc/jap/122/3
Published by the American Institute of Physics

Conducting wall Hall thrusters in magnetic shielding and standard configurations

Lou Grimaud[a] and Stéphane Mazouffre
Electric Propulsion Team, ICARE, CNRS, Orléans, France

(Received 14 April 2017; accepted 9 July 2017; published online 21 July 2017)

Traditional Hall thrusters are fitted with boron nitride dielectric discharge channels that confine the plasma discharge. Wall properties have significant effects on the performances and stability of the thrusters. In magnetically shielded thrusters, interactions between the plasma and the walls are greatly reduced, and the potential drop responsible for ion acceleration is situated outside the channel. This opens the way to the utilization of alternative materials for the discharge channel. In this work, graphite walls are compared to BN-SiO_2 walls in the 200 W magnetically shielded ISCT200-MS and the unshielded ISCT200-US Hall thrusters. The magnetically shielded thruster shows no significant change in the discharge current mean value and oscillations, while the unshielded thruster's discharge current increases by 25% and becomes noticeably less stable. The electric field profile is also investigated through laser spectroscopy, and no significant difference is recorded between the ceramic and graphite cases for the shielded thruster. The unshielded thruster, on the other hand, has its acceleration region shifted 15% of the channel length downstream. Lastly, the plume profile is measured with planar probes fitted with guard rings. Once again the material wall has little influence on the plume characteristics in the shielded thruster, while the unshielded one is significantly affected. *Published by AIP Publishing.*
[http://dx.doi.org/10.1063/1.4995285]

I. INTRODUCTION

A. Hall thrusters (HT)

Hall thrusters (HT) are the most used plasma propulsion systems for spacecraft.[1] They combine high power to thrust ratio with good efficiency and a specific impulse range well suited for earth orbit operations. Their traditional role has been in station keeping of geostationary satellites with a discharge power around 1 kW. However, new applications and needs have emerged for electric propulsion. On one end of the spectrum, low power thrusters ranging from a few tens to a few hundred watts are required for small satellite applications where propulsion is a challenge. The higher power range is also full development with power requirements in the order of 5 to 10 kW for orbit transfer of heavier geostationary satellites or for explorations missions.[2]

In order for Hall thrusters to be competitive in those applications, one limitation is their lifespan. Magnetic shielding (MS) magnetic configuration promises longer lifespan with minimal changes from the traditional thruster.

B. Conducting wall thrusters

Since the Hall thruster technology emerged from the Soviet Union, the material of choice for the discharge channel has been boron nitrite (BN) compounds. Most thruster uses BN HP (95% BN with a calcium borate binder), BN M26 (40% BN, 60% SiO_2), or the Russian Borosil (49% BN, 49% SiO_2, 1% Y_2O_3). Those materials offer similar thruster performances.[3,4] However, additives such as silicon nitride and aluminum nitride can degrade performance by modifying the secondary electron emission (SEE) behavior of the walls.[5]

Data on the performance of Hall thrusters with alternative materials are less common. Raitses and Ashkenazy performed some performance measurements with machinable glass ceramics,[6,7] which showed a considerable performance degradation. A large electron current is measured which lowers the efficiency of the thruster. Tests with alumina walls have shown a similar behavior as well as the modification of the acceleration region.[8,9] Raitses conducted a number of studies with thin conducting rings made of graphite and carbon velvet.[10–19] Those highlight the importance of the SEEs on the thruster performance. They also show how conducting materials can change the position of the electric field. Diamond was tested in Stanford's linear Hall thruster.[20] This open drift geometry is not easily compared to classical Hall thrusters and the diamond walls induced very unstable operation under 200 V. A micro Hall thruster with alumina and diamond surfaces was also fired at Stanford, but the setup was far from the conventional HT.[21]

The most complete study up to date was done by Gascon in the early 2000s.[22,23] A full set of performance measurements with BN-SiO_2, Al_2O_3, SiC, and graphite were performed. The boron nitride showed the best performance by far in terms of stability, operating range, and thruster efficiency. Interestingly, the thrust measured seemed only weakly affected by the wall material. The material effects were principally seen on the discharge current means value and oscillations. Those differences were explained by an

[a]Electronic mail: lou.grimaud@cnrs-orleans.fr.

increase in the electron current to the anode caused by the change in secondary electron emission properties of the walls.

More recently, Goebel *et al.*, taking into account the reduced interaction between the walls and the plasma, as well as the constant plasma potential along the walls in magnetic shielded thrusters, tested graphite walls.[24] The magnetically shielded H6-MS showed only minor differences in performances and operated at the same current and with the same dynamics with BN or graphite walls.

It is important to note that those experiments with conducting walls are not equivalent to thrusters with anode layers (TAL). In most cases, the walls are left floating with respect to the anode and the cathode, whereas in a TAL, the ring situated at the exit plane is at the cathode potential.[25]

C. Magnetic shielding

Magnetic shielding (MS) refers to a specific magnetic topology initially developed by JPL.[26–31] It has been shown to greatly reduce the erosion of the Hall thruster wall while conserving similar performances to unshielded (US) thrusters.

The basic principle relies on the high electron mobility along the magnetic field lines, which makes the plasma potential as well as the electron temperature quasi-constant along them.[32] Figure 1 illustrates how magnetic field lines tangent to the walls of the thruster (the so-called "grazing lines") effectively shield the walls from the plasma. Two effects are at play in the magnetically shielded Hall thruster (MS-HT). First, the fact that the magnetic field lines do not connect directly to the walls means that there is no strong acceleration electric field along them, and that the ions stay slow in their vicinity. The second effect is that a layer of cold electrons is created near the walls and reduces the sheath energy. Both those effects contribute to a lower average energy of the ions, impacting the walls and thus less sputtering.[33]

As illustrated in Fig. 1, contrary to standard unshielded thrusters, there is a little potential drop along the walls of a shielded thruster. Moreover, the electron temperature being low means that secondary electron emissions are not as frequent as in US-HT. This realization prompted Goebel *et al.* to try to replace the walls of the H6-MS shielded thruster with graphite.[24]

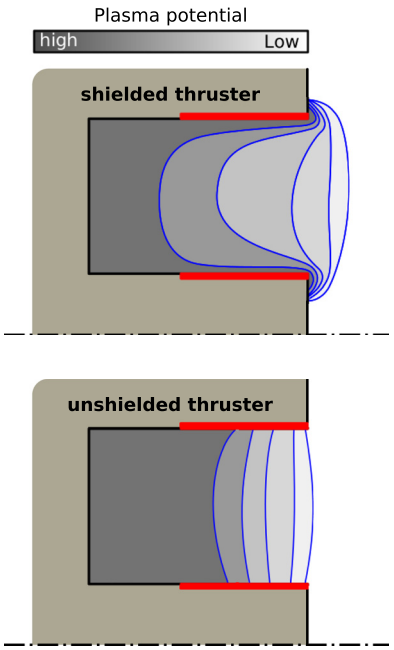

FIG. 1. Configuration of the shielded and unshielded thrusters. The magnetic field lines are represented in blue. The grayscale gradient represents the plasma potential. The position of the graphite inserts is in red.

II. EXPERIMENTAL SETUP

A. Test facility

All the experiments have been conducted in the NExET (New Experiments in Electric Propulsion) test chamber. The setup consists in a $1.8 \times 0.8\varnothing$ m stainless steel vacuum vessel fitted with a large dry pump, a 350 l/s turbo-molecular pump, and a cryogenic pump cooled down to approximately 30 K. The pumping system allows for operation between 5 and 9×10^{-5} mbar at the operating points described in this paper.

B. Thrusters

In order to compare the effect of conducting graphite walls on both regular and magnetically shielded thrusters small 200 W permanent magnets Hall thrusters were used. The ISCT200-US is a standard unshielded (US) thruster usually fitted with a BN-SiO_2 discharge channel. The ISCT200-MS is a magnetically shielded thruster (MS) that shares the same channel geometry as well as the same magnetic field profile and intensity at the center of the discharge channel. This was done on purpose to compare the performances of small US and MS thrusters. The shape of the magnetic field profile in both thrusters is represented in Fig. 2.

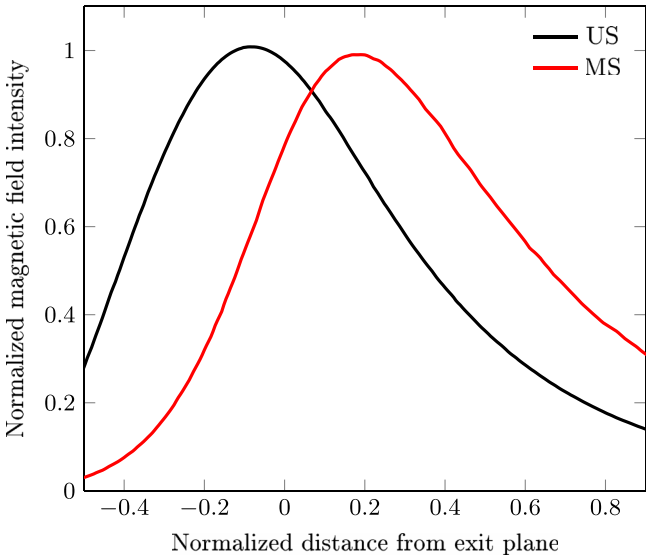

FIG. 2. Magnetic field intensity along the center of the discharge channel for the ISCT200-US and ISCT200-MS. The field intensity is normalized by the maximum field intensity at the center of the discharge channel, and the distance is normalized by its length.

Both thrusters share similar discharge characteristics near their 200 V, 1 mg/s xenon mass flow nominal discharge point. More details on the differences and similarities between both thrusters and performance comparisons are available in previous publications.[33–35]

A special set of discharge channel walls were built to investigate the effects of conducting walls on the thruster performances. Figure 3 shows the thin graphite inserts before firing. Those inserts are insulated from the anode and are left electrically floating with respect to the other components of the thrusters. The graphite is a fine grain isostatically pressed grade and has an electrical resistivity of 14 $\mu\Omega$m.

The MS thruster was fired with clean new BN-SiO_2 walls and graphite walls. The US-HT was fired with used BN-SiO_2 walls and graphite walls. Each thruster was left under vacuum for at least 12 hours and fired one hour in order to outgas the new components. Before data acquisition started we waited 30 minutes for thermal stabilization.

The discharge current was recorded with a Tektronix current probe (TCP202, dc to 50 MHz bandwidth). The probe was connected to a Tektronix digital oscilloscope (TDS5104, 1 GHz, 5GS/s) to monitor and record the electrical signals at a sampling rate of 2.5 MHz.

C. Electric field determination

The position and intensity of the axial electric field were measured via laser induced fluorescence spectroscopy (LIF). This technique allows us to measure the ion velocity distribution functions (IVDF) and compute the electric field responsible for their change. This method has no measurable disturbing effect on the discharge contrary to emissive or Langmuir probes.[36–38]

A narrow-band tunable diode laser is used to pump the $5d^4F_{7/2} \rightarrow 6p^2D^0_{5/2}$ metastable Xe^+ ion transition. Those excited ions then relax down to their ground energy level by emitting fluorescent photons at 541.9 nm. This fluorescence light is collected though a fiber and fed through a monochromator to isolate it from other spontaneous light emissions. The light intensity is then measured by a photomultiplier.

FIG. 3. Discharge channel with the graphite inserts. The graphite inserts cover two thirds of the discharge channel length.

The fast metastable ions experience a Doppler shift relative to the stationary laser. This means that by tuning the laser wavelength, different velocity groups of ions can be excited. The intensity of the fluorescence signal lets us measure their relative density and trace the IVDF.

For this study, the laser measures the axial velocity component of the ions and goes through the center of the discharge channel. More details on the LIF optical setup can be found in the literature.[39]

From the IVDFs measured at different positions along this axis, we can compute the axial electric field responsible for the ion acceleration. The potential drop (V) experienced by the ions can be calculated by considering their kinetic energy corresponding to their most probable velocity (v_{mp}) as explained in Eq. (1)

$$V = \frac{m_{Xe} \cdot v_{mp}^2}{2e}, \tag{1}$$

with e being the ion charge in Coulombs and m_{Xe} the xenon ion mass.

The electric field is then computed with a second order centered difference scheme.

Other more complex methods exit to compute the electric field from the IVDF; however, they are more sensitive to noise and thus are not necessarily more accurate in practice.[40]

D. Plume diagnostics

Plume measurements were performed with a 5.6 mm diameter stainless steel planar probe fitted with a guard ring. The probe was polarized to −30 V and swept in front of the thruster over a 180 degrees, 68 cm diameter arc. The collected current is measured with a Keithley 2410 sourceMeter. More details on the system can be found in the literature.[34]

Testing at different probe voltages shows no difference in the collected current. This indicates that the guard ring successfully maintains a flat sheath across the collecting surface.

In order to compensate for charge exchange effects, the non-zero current collected at 90 degrees from the thruster was subtracted from the current density profiles before computing the divergence angle, beam current efficiency, and propellant utilization efficiency. Since no data are available at the moment on the ion fraction in the plume of the ISCT200-MS and ISCT200-US, no correction was applied for the presence of multiply charged ions. This processing is somewhat basic but is only intended as a mean of comparing the two thrusters at hand.

In this study, we considered the divergence angle as the half angle containing 90% of the collected current over the hemisphere facing the thruster. The beam efficiency is defined as the ratio of ion current collected over the power supply discharge current. The propellant utilization efficiency is defined as the ratio of the quantity of collected ions

(assuming they are only simply charged) over the quantity of neutral xenon atoms injected.

III. RESULTS

A. Discharge parameters

1. Envelope and discharge current

The mean discharge current for different xenon mass flow and voltages is presented in Fig. 4 for the US-HT and in Fig. 5 for the MS-HT. The conducting walls increase the discharge current by 15% to 30% in the unshielded thruster when the discharge voltage is kept below 350 V. For the MS-HT, the discharge characteristics between 150 and 300 V are very similar with the two materials. The graphite slightly reduces the discharge current but by no more than 10%.

At high discharge powers, operation is usually limited by the apparition of hot spots in the discharge channel. After those hot spots appear, we usually observe a slow but steady increase in the discharge current even though the voltage is maintained constant. With the graphite walls in the shielded thruster, this behavior is not observed. The current remains stable and the thruster was operated for more than 15 min at nearly 400 W without any issue. Operation above 400 V was limited by the maximum range of the power supply.

2. Discharge stability

Figures 4 and 5 show not only the mean discharge current but also the amplitude of the current oscillations. The filled in area corresponds to where the current is 90% of the time. The 90% threshold is taken in order to minimize the influence of potentially irregular current spikes or dips.

The unshielded and shielded thrusters with BN-SiO_2 walls exhibit a typical stability range with oscillations at low

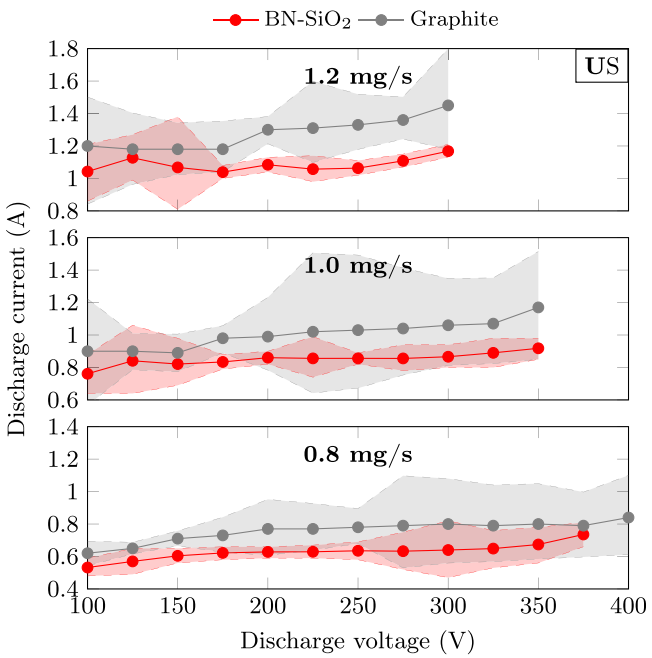

FIG. 4. Discharge current for the US thruster with ceramic walls and graphite walls. The filled in areas delimit the top 10% and bottom 10% of the current oscillations are at this operating point.

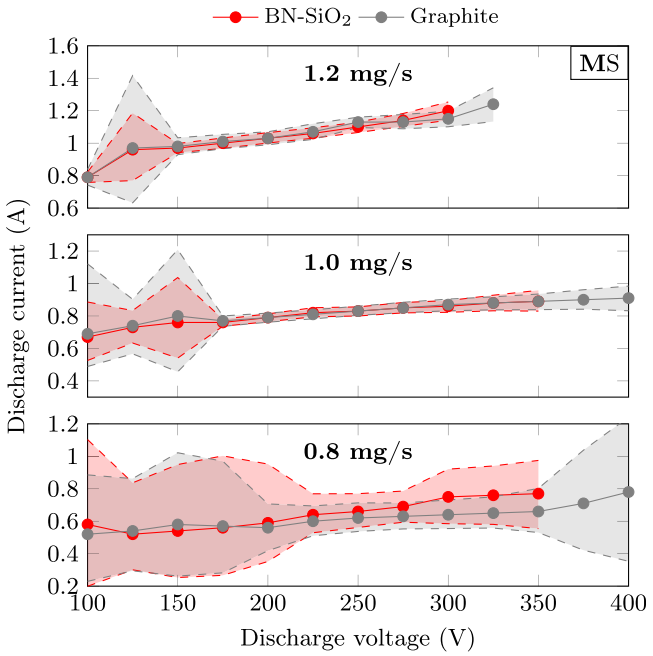

FIG. 5. Discharge current for the MS thruster with ceramic walls and graphite walls. The filled in areas delimit the top 10% and bottom 10% of the current oscillations are at this operating point.

voltages ($\leq$ 150 V) and a stable zone between 175 and 250 V before oscillations start to slowly increase at higher voltages.

With the graphite walls, the US-HT is nearly always less stable than its ceramics counterpart. The current oscillations at high voltage appear sooner and are more pronounced. However in the magnetically shielded case, the differences are minimal. The transitions follow the same pattern and have the same amplitude as with the ceramics for the mass flow of 1.0 and 1.2 mg/s or xenon. For the lower 0.8 mg/s mass flow, the graphite even reduces the oscillations.

Figures 6 and 7 represent the power spectra (Welch's method) of the current for different discharge voltages at 1 mg/s of xenon mass flow. Once again the difference the material makes in the US thruster is clearly visible. From 200 to 350 V a clear main frequency emerges between 10 and 20 kHz in the graphite case. A similar peak is visible around 40 kHz at 225 V in the ceramics US case but becomes more diffuse at higher voltages. This is consistent with the results of Gascon in the unshielded SPT-100-ML.[22,23]

Both shielded cases are similar. The low voltage oscillations are localized between 10 and 20 kHz, but after reaching 175 V, the spectrum flattens considerably. The increased oscillations at higher voltages engulf a wide range of frequencies between 5 and 50 kHz. The two characteristic frequencies at 8 and 70 kHz observed by JPL on the H6-MS at 300 V are not seen here.[24]

B. Electric field distribution

The LIF spectroscopy acquisitions were performed at 200 V and 1 mg/s which we define as our nominal operating point. The electric field computed from the IVDFs is presented in Fig. 8. The position is normalized by the discharge channel length.

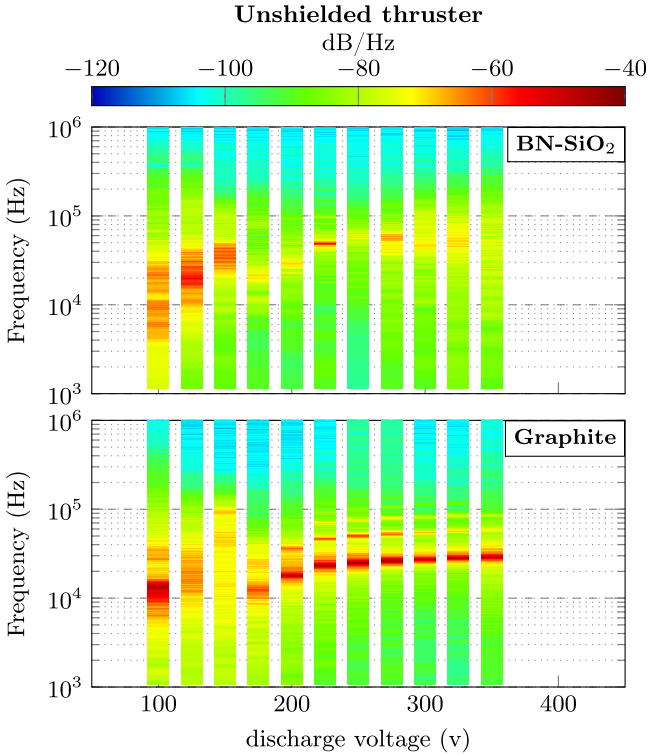

FIG. 6. Spectra of the discharge current for the US-HT with BN-SiO_2 (top) and graphite (bottom) walls for a range of discharge voltages at 1 mg/s.

Classically in the US and MS Hall thrusters, the electric field is positioned near the maximum magnetic field.

The measurements show a clear effect of the conducting walls on the unshielded thruster. While the field maximum intensity remains similar, the electric field position is around

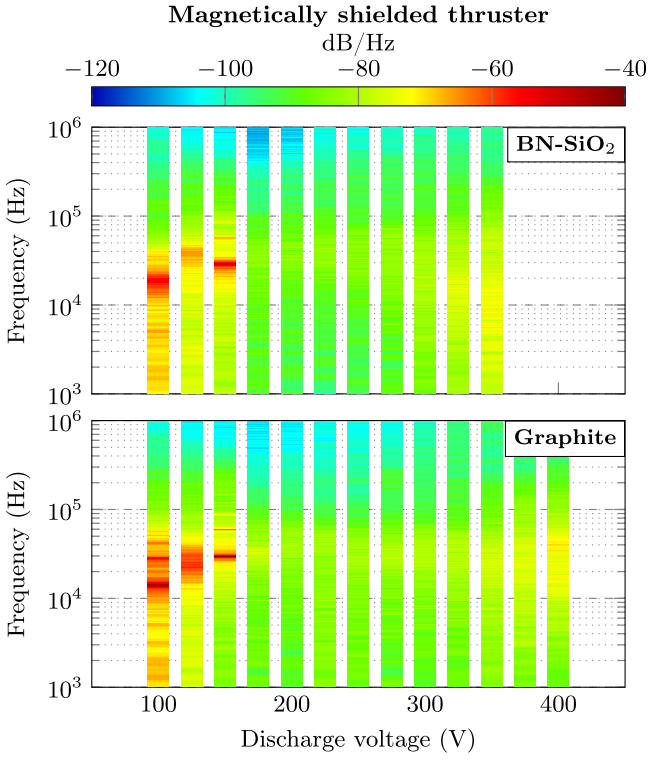

FIG. 7. Spectra of the discharge current for the MS-HT with BN-SiO_2 (top) and graphite (bottom) walls for a range of discharge voltages at 1 mg/s.

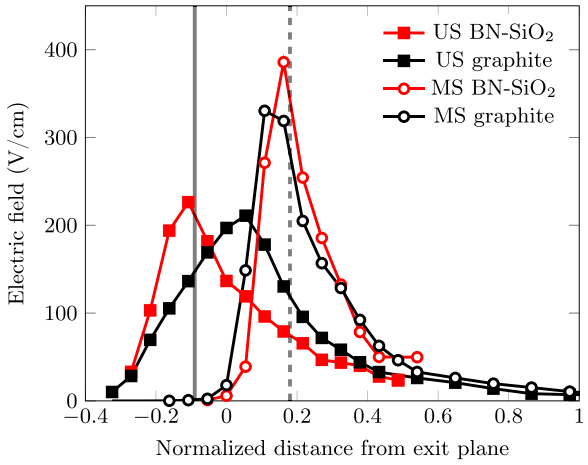

FIG. 8. Electric field position as a function of the distance from the exit plane. The vertical lines represent the position of the maximum of the magnetic field for the US-HT (continuous line) and MS-HT (dashed line).

20% of the discharge channel length further downstream. It also does not correspond to the maximum magnetic field anymore.

In the MS-HT, the wall material doesn't affect the acceleration region in any appreciable way. The slight shift upstream is within the absolute position error of the optical system.

The final velocity of the ion is weakly affected by the change of material. The BN achieves 15700 m/s, while the graphite had a slightly higher 15840 m/s final velocity in the shielded thruster. In the US case, the final velocity for graphite is 15800 m/s and 15400 m/s for BN.

The displacement of the electric field downstream is somewhat contrary to what was measured by Raitses with graphite[18] and carbon-velvet[10] (a conducting material with no secondary electron emissions). It is worth noting that in those experiments, the conducting segments spanned only about 10% of the discharge channel compared to 60% in the ISCT200-MS and ISCT200-US. The measurements were also performed with emissive probes, which are known to disturb the discharge.[36,37]

C. Plume characteristics

The current density profiles collected by the planar probe with guard ring are presented in Fig. 9. Those are not corrected for charge exchange or background plasma. Even just considering those profiles, it can easily be seen how the shielded thruster plume is not affected by the change of wall material, while the unshielded thruster plume widens significantly when switching to the graphite walls.

Table I shows the calculated divergence angle, beam current efficiency, and propellant utilization efficiency. As previously shown, with ceramics walls the US-HT and MS-HT have similar divergence angle and beam efficiency. The MS-HT is 6 to 7% less propellant efficient than the US-HT at similar discharge voltage and mass flow rate.

The switch to graphite walls does not change the MS-HT performances. The calculated efficiencies increase by only 2% or less and the divergence angle stays the same. In the US-HT, however the conducting walls increase the divergence at 200 V

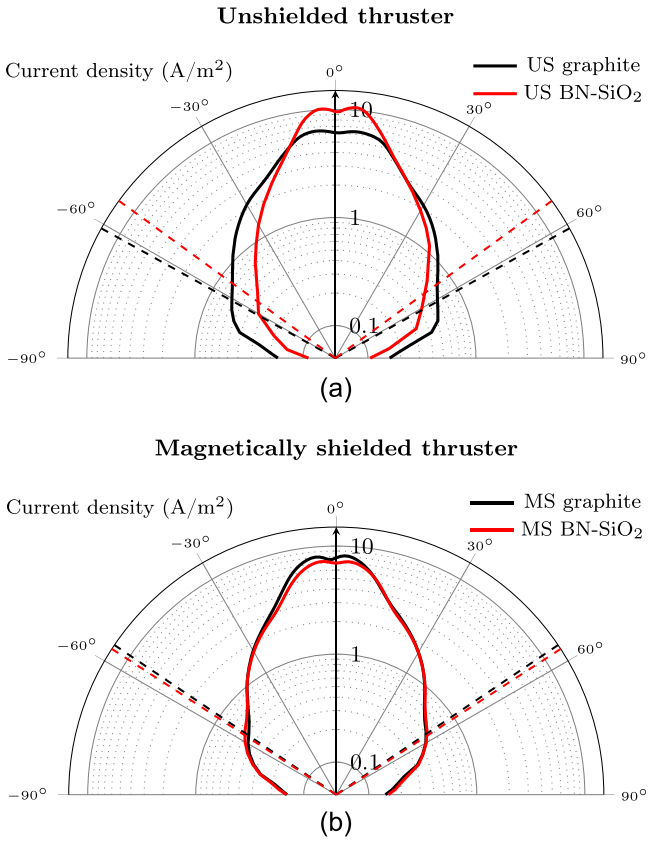

FIG. 9. Current density profiles measured across the plume with planar probes with guard rings at 200 V and 1 mg/s of xenon for the US-HT (top) and MS-HT (bottom). The dashed lines represent the divergence angle for the BN-SiO_2 (red) and graphite cases (black).

and the computed propellant utilization at both voltages. Beam efficiency does not appear to be affected.

A propellant utilization efficiency of 100% as seen in the unshielded thruster with graphite walls is highly suspicious. This is a result of the rather simple data processing done here. Offsetting the discharge current by the background measured at high angle (as described in part 2.4) does not account for all charge exchange phenomena, multiply charged ion fractions, or pressure effects. The data presented here are mostly useful as a qualitative comparison between measurements performed with the same system, in the same facility, and with similar thrusters.

IV. DISCUSSION

A. Wall materials and Hall thruster physics

As far as thruster characteristics are concerned the change from BN-SiO_2 to graphite as two main consequences.

First the discharge channel is switched from a dielectric to a conducting material. This means that any potential difference along the walls can be short-circuited through the wall material. As discussed in part 1.3, the grazing line along the walls limits the potential gradient along the walls in MS-HT. This makes it less likely to have significant currents going through them. In US-HT, the electric field is usually located at the same axial position as where we set up the graphite inserts (see Fig. 8). This makes the electron likely to bypass the magnetic barrier by going through the walls. It seems that as a result, the potential gradient relocates downstream. This push of the acceleration region downstream could explain the higher divergence and will probably lead to lower thrust performances.

The second difference between boron nitride compound and graphite is their secondary electron emission properties. The secondary electron emission yield of BN-SiO_2 reaches unity near 40 eV (Refs. 41–43), while it is always below 0.8 even at 100 eV for graphite.[44,45] This has a major influence on the plasma in the acceleration region of unshielded thrusters where the hot (around 30 eV) electron population is in contact with the walls. The SEEs are one of the key factors in the electron energy balance, and thus the thruster performances.[46–48] The mechanism by which they influence the transport across the magnetic barrier is not yet well understood.[49–51] However, it appears that BN compounds have ideal SEE characteristics for Hall thruster discharge. Tests with higher SEE yield materials such as alumina do not have as good performances as boron nitride.

The study of SEE yield effects on Hall thruster performances has traditionally been complicated.

First, the actual SEE properties for dielectric material are not easily measurable and are often done at energies, current density, and temperatures far from those encountered in Hall thrusters. While σ for BN-SiO_2 is often reported to be close to unity in typical Hall thruster conditions, it is less well known that this coefficient decreases significantly when the temperature of the BN compound is increased. Belhaj *et al*. report a 40% decrease in the first cross-over energy at 400 °C.[52] This temperature only represents the lower end of the typical operating temperature for Hall thruster ceramics.[53] The current density[43] and the incidence angle of the electron beam[54] also have significant effects on the measured values. This illustrates how much uncertainty exists in the SEE and thus to its contribution to the bulk electron properties.

Attempts have been made to suppress SEE by replacing the boron nitride with other materials. Apart from diamond, no other low SEE yield temperature resistant dielectric

TABLE I. Overview of the data derived from plume measurements. All the cases presented were done at a mass flow of 1 mg/s of xenon.

		BN-SiO_2			Graphite		
	Vd (V)	Divergence (deg)	Beam efficiency	Propellant utilization	Divergence (deg)	Beam efficiency	Propellant utilization
MS	200	57	66%	70%	56	68%	72%
	300	57	63%	75%	57	65%	77%
US	200	54	66%	77%	62	65%	91%
	300	58	64%	81%	60	66%	100%

material is readily available. When using conducting materials such as graphite, or the very low SEE yield carbon-velvet, it is nearly impossible to decouple the effect of SEE from the effects of a conducting channel.

Interestingly, the results presented here show that the wall material has a very little effect on a MS-HT. This points toward a greatly reduced plasma/wall interaction. Why then, are shielded Hall thruster characteristics so close to unshielded thrusters with BN walls?[34,55] The near absence of interactions between the plasma and the wall should effectively emulate a classical unshielded thruster with zero secondary electron emissions. The SEE yield σ of BN in US-HT could be overestimated due to the measuring techniques employed and or not taking into account temperature and incidence angle effects. The similarities could also be explained by different energy loss mechanisms for the electrons. Instead of cooling down during their collisions with the walls, the high energy electrons contribute to the creation of Xe^{2+} and Xe^{3+} ions. High fractions of multicharged ions have been measured in MS-HT.[29]

An interesting test to see if MS-HT are truly material agnostic would be to use a higher SEE yield material such as alumina.[43]

B. Conducting walls in magnetically shielded thrusters

MS-HT promise considerably increased lifespans for Hall thrusters while keeping similar performances to the unshielded counterparts. However, they face specific challenges for ground testing and qualification. One of these issues is deposition of the material sputtered from the vacuum chamber walls. This material (often mostly carbon from graphite protection screens) creates a black conducting layer on the thruster surfaces not subjected to erosion. In unshielded thruster, this deposit layer is eroded away at the exit of the discharge channel keeping the ceramic exposed.

In MS thrusters, where the erosion rate is lower than the deposition rate, the carbon layer tends to accumulate in the discharge channel. It changes channel material properties and is not representative of what is happening in operation in space. This is not compatible with the "test as you fly" philosophy of space hardware qualification. Showing that changing the wall material has little effect on the performances is a good indication that the deposition would have a minimal impact on the thruster. Initially designing an MS thruster with graphite walls would also make this carbon deposition process less of a change in wall properties. Incidentally, tests in our facility have shown that the gradual buildup of the carbon layer on the ISCT200-MS ceramic walls had no appreciable effects on the discharge.

Lastly, BN is a brittle material and is hard to machine (hence the addition of silica). If MS-HT are truly not affected by the wall material, tougher ceramics or even metals could be used. Replacement materials would need to be heat resistant up to around 600 °C and not disturb the magnetic field. Metals such as stainless steel or titanium could be good candidates for such applications. The use of such readily available and easier to machine materials would reduce thruster cost.

V. CONCLUSION

This works shows that the magnetic shielding topology allows the use of graphite walls, and presumably other materials, in Hall thrusters without significantly changing the discharge characteristics. This confirms the results obtained by Goebel *et al*. and extends them to low power thrusters.[24] Direct comparisons between shielded and unshielded thrust highlight the fact that this is only achievable thanks to the specific conditions created by the magnetic shielding topology.

These results also pose interesting questions on the effect of secondary electron emissions in Hall thrusters. Since SEEs have important effects on the anomalous transport of electrons, one can wonder how different this mechanism is between unshielded and shielded thrusters.

ACKNOWLEDGMENTS

We are indebted to Julien Vaudolon who developed and tested the first version of the ISCT200-MS, for his insightful advices and many discussions we had on the concept of magnetic shielding. We also like to thank Sedina Tsikata for her help on understanding the phenomenon related to secondary electron emission in Hall thrusters.

We also like to thank the reviewers, particularly for their helpful comments on secondary electron emissions.

This work was done as part of the CNES research program. It has been financially supported by the CNES and the Région Centre council.

[1]J.-P. Boeuf, "Tutorial: Physics and modeling of Hall thrusters," J. Appl. Phys. **121**(1), 011101 (2017).
[2]S. Mazouffre, "Electric propulsion for satellites and spacecraft: Established technologies and novel approaches," Plasma Sources Sci. Technol. **25**(3), 033002 (2016).
[3]P. Peterson, D. Manzella, and D. Jacobson, "Investigation of the erosion characteristics of a laboratory Hall thruster," AIAA Paper No. 2003-5005, 2003.
[4]R. Eytan, D. Lev, G. Alon, A. Warshavsky, A. Kapulkin, and M. Rubanovitz, "Wall material selection process for CAM200 low power Hall thruster," in Joint Conference of 30th International Symposium on Space Technology and Science 34th International Electric Propulsion Conference and 6th Nano-Satellite Symposium, Hyogo-Kobe, Japan (2015).
[5]H. Tahara, K. Imanaka, and S. Yuge, "Effects of channel wall material on thrust performance and plasma characteristics of Hall-effect thrusters," Vacuum **80**(11-12), 1216–1222 (2006).
[6]Y. Raitses, J. Ashkenazy, G. Appelbaum, and M. Guelman, "Experimental investigation of the effect of channel material on Hall thruster characteristics," in 25th International Electric Propulsion Conference, Cleveland, OH, USA (1997).
[7]J. Ashkenazy, Y. Raitses, and G. Appelbaum, "Parametric studies of the Hall thruster at Soreq," Israel Atomic Energy Commission 1997 Annual Report, 1997, pp. 66–93; https://www.iaea.org/inis/collection/NCLCollectionStore/_Public/30/023/30023822.pdf.
[8]N. Gascon and M. A. Cappelli, "Wall effects on the excitation and propagation of instabilities in Hall thrusters," in 28th International Electric Propulsion Conference (2003), Vol. **3032**, pp. 1–10.
[9]J. Vaudolon, "Electric field determination and magnetic topology optimization in Hall thrusters," Ph.D. thesis (Université d'Orléans, 2015).
[10]Y. Raitses, I. D. Kaganovich, A. Khrabrov, D. Sydorenko, N. J. Fisch, and A. Smolyakov, "Effect of secondary electron emission on electron cross-

field current in E X B discharges," IEEE Trans. Plasma Sci. **39**(4), 995–1006 (2011).
[11]Y. Raitses, D. Staack, and N. Fisch, "Controlling the plasma potential distribution in segmented-electrode Hall thruster," IEEE Trans. Plasma Sci. **36**(4), 1202–1203 (2008).
[12]Y. Raitses, D. Staack, M. Keidar, and N. J. Fisch, "Electron-wall interaction in Hall thrusters," Phys. Plasmas **12**, 57104 (2005).
[13]K. D. Diamant, J. E. Pollard, R. B. Cohen, Y. Raitses, and N. J. Fisch, "Segmented electrode hall thruster," J. Propul. Power **22**(6), 1396–1401 (2006).
[14]Y. Raitses, A. Smirnov, D. Staack, and N. J. Fisch, "Measurements of secondary electron emission effects in the Hall thruster discharge," Phys. Plasmas **13**(1), 014502 (2006).
[15]Y. Raitses, D. Staack, A. Dunaevsky, and N. J. Fisch, "Operation of a segmented Hall thruster with low-sputtering carbon-velvet electrodes," J. Appl. Phys. **99**(3), 036103 (2006).
[16]Y. Raitses, A. Smirnov, N. Fisch, and D. Staack, "Segmented electrodes in annual and cylindrical Hall thrusters," AIAA Paper No. 2006-4471, 2006.
[17]Y. Raitses, D. Staack, L. a. Dorf, and N. J. Fisch, "Controlling ion acceleration region in Hall thrusters," in *Proceedings of the International Electric Propulsion Conference 2005 (IEPC05)* (2005), pp. 29–32.
[18]Y. Raitses, M. Keidar, D. Staack, and N. J. Fisch, "Effects of segmented electrode in Hall current plasma thrusters," J. Appl. Phys. **92**(9), 4906–4911 (2002).
[19]Y. Raitses, L. A. Dorf, A. A. Litvak, and N. J. Fisch, "Plume reduction in segmented electrode Hall thruster," J. Appl. Phys. **88**(3), 1263–1270 (2000).
[20]N. B. Meezan, N. Gascon, and M. A. Cappelli, "Linear geometry Hall thruster with boron nitride and diamond walls," in *27th International Electric Propulsion Conference, Pasadena, CA, USA* (2001), pp. 15–19.
[21]T. Ito, N. Gascon, W. S. Crawford, and M. A. Cappelli, "Experimental characterization of a micro-Hall thruster," J. Propul. Power **23**(5), 1068–1074 (2007).
[22]N. Gascon, M. Dudeck, and S. Barral, "Wall material effects in stationary plasma thrusters. I. Parametric studies of an SPT-100," Phys. Plasmas **10**(10), 4123–4136 (2003).
[23]N. Gascon, "Etude de propulseurs plasmiques à effet Hall pour systèmes spatiaux: performances, propriétés des décharges et modélisation hydrodynamique," Ph.D. thesis (Aix-Marseille, 2000).
[24]D. M. Goebel, R. R. Hofer, I. G. Mikellides, I. Katz, J. E. Polk, and B. N. Dotson, "Conducting Wall Hall thrusters," IEEE Trans. Plasma Sci. **43**(1), 118–126 (2015).
[25]E. Y. Choueiri, "Fundamental difference between the two Hall thruster variants," Phys. Plasmas **8**(11), 5025 (2001).
[26]I. Mikellides, I. Katz, R. Hofer, D. Goebel, K. de Grys, and A. Mathers, "Magnetic shielding of the acceleration channel walls in a long-life Hall thruster," AIAA Paper No. 2010–6942, 2010.
[27]I. G. Mikellides, I. Katz, R. R. Hofer, D. M. Goebel, K. de Grys, and A. Mathers, "Magnetic shielding of the channel walls in a Hall plasma accelerator," Phys. Plasmas **18**(3), 033501 (2011).
[28]I. Mikellides, I. Katz, and R. Hofer, "Design of a laboratory Hall thruster with magnetically shielded channel walls, Phase I: Numerical simulations," in 47th AIAA/ASME/SAE/ASEE Joint Propulsion Conference & Exhibit, 2011, No. August, pp. 1–18.
[29]R. Hofer, D. Goebel, I. Mikellides, and I. Katz, "Design of a laboratory Hall thruster with magnetically shielded channel walls, Phase II: Experiments," AIAA Paper No. 2012-3788, 2012.
[30]I. Mikellides, I. Katz, R. Hofer, and D. Goebel, "Design of a laboratory Hall thruster with magnetically shielded channel walls, Phase III: Comparison of theory with experiment," AIAA Paper No. 2012-3789, 2012.
[31]I. G. Mikellides, I. Katz, R. R. Hofer, and D. M. Goebel, "Magnetic shielding of walls from the unmagnetized ion beam in a Hall thruster," Appl. Phys. Lett. **102**(2), 023509 (2013).
[32]A. I. Morozov and V. V. Savelyev, *Fundamentals of Stationary Plasma Thruster Theory*, Reviews of Plasma Physics Vol. 21 (Springer US, 2000), pp. 203–391.
[33]L. Grimaud and S. Mazouffre, "Ion behavior in low-power magnetically shielded and unshielded Hall thrusters," Plasma Sources Sci. Technol. **26**(5), 055020 (2017).
[34]L. Grimaud, J. Vaudolon, S. Mazouffre, and C. Boniface, "Design and characterization of a 200W Hall thruster in "magnetic shielding" configuration," AIAA Paper No. 2016-4832, 2016.
[35]L. Grimaud, J. Vaudolon, and S. Mazouffre, "Design and characterization of a 200 W low power Hall thruster in "magnetic shielding" configuration," Space Propulsion Conference, Rome (2016).
[36]L. Grimaud, A. Pétin, J. Vaudolon, and S. Mazouffre, "Perturbations induced by electrostatic probe in the discharge of Hall thrusters," Rev. Sci. Instrum. **87**(4), 043506 (2016).
[37]D. Staack, Y. Raitses, and N. Fisch, "Investigations of probe induced perturbations in a Hall thruster," AIAA Paper No. 2002-4109, 2002.
[38]B. Jorns, D. M. Goebel, and R. R. Hofer, "Plasma perturbations in high-speed probing of Hall thruster discharge chambers: Quantification and mitigation," AIAA Paper No. 2015-4006, 2015.
[39]S. Mazouffre, "Laser-induced fluorescence diagnostics of the cross-field discharge of Hall thrusters," Plasma Sources Sci. Technol. **22**(1), 013001 (2013).
[40]J. Vaudolon and S. Mazouffre, "Indirect determination of the electric field in plasma discharges using laser-induced fluorescence spectroscopy," Phys. Plasmas **21**(9), 093505 (2014).
[41]V. Viel-Inguimbert, "Secondary electron emission of ceramics used in the channel of SPT," in *28th International Electric Propulsion Conference, Toulouse, France* (2003), pp. IEPC–2003–I258.
[42]A. Dunaevsky, Y. Raitses, and N. J. Fisch, "Secondary electron emission from dielectric materials of a Hall thruster with segmented electrodes," Phys. Plasmas **10**(6), 2574–2577 (2003).
[43]T. Tondu, M. Belhaj, and V. Inguimbert, "Electron-emission yield under electron impact of ceramics used as channel materials in Hall-effect thrusters," J. Appl. Phys. **110**(9), 093301 (2011).
[44]J. M. Pedgley and G. M. McCracken, "Plasma sheath properties calculated using measured secondary electron emission coefficients," Plasma Phys. Controlled Fusion **35**(3), 397–409 (1993).
[45]M. Belhaj, J. Roupie, O. Jbara, J. Puech, N. Balcon, and D. Payan, "Electron emission at very low electron impact energy: Experimental and Monte-Carlo results," in Proceedings of ECLOUD'12, 2013, Vol. CERN-2013, No. 2, p. 137.
[46]E. Ahedo, J. M. Gallardo, i. Mart, and M. Sánchez, "Effects of the radial plasma-wall interaction on the Hall thruster discharge," Phys. Plasmas **10**(8), 3397–3409 (2003).
[47]S. Barral, K. Makowski, Z. Peradzynski, N. Gascon, and M. Dudeck, "Wall material effects in stationary plasma thrusters. II. Near-wall and in-wall conductivity," Phys. Plasmas **10**(10), 4137 (2003).
[48]L. Garrigues, G. J. M. Hagelaar, C. Boniface, and J. P. Boeuf, "Anomalous conductivity and secondary electron emission in Hall effect thrusters," J. Appl. Phys. **100**(12), 123301 (2006).
[49]A. Héron and J. C. Adam, "Anomalous conductivity in Hall thrusters: Effects of the non-linear coupling of the electron-cyclotron drift instability with secondary electron emission of the walls," Phys. Plasmas **20**(8), 082313 (2013).
[50]D. Sydorenko, A. Smolyakov, I. Kaganovich, and Y. Raitses, "Kinetic simulation of secondary electron emission effects in Hall thrusters," Phys. Plasmas **13**(1), 014501 (2006).
[51]F. Taccogna, P. Minelli, M. Capitelli, and S. Longo, "Physics of Hall-effect thruster by particle model," in *28th International Symposium on Rarefied Gas Dynamics 2012* (AIP Publishing, 2012), Vol. 1501, pp. 1390–1399.
[52]M. Belhaj, N. Guibert, K. Guerch, P. Sarrailh, and N. Arcis, "Temperature effect on the electron emission yield of BN-SI02 under electron irradiation," in Spacecraft Charging Technology Conference 2014 (13th SCTC), Pasadena, USA (2014).
[53]S. Mazouffre, P. Echegut, and M. Dudeck, "A calibrated infrared imaging study on the steady state thermal behaviour of Hall effect thrusters," Plasma Sources Sci. Technol. **16**(1), 13–22 (2007).
[54]N. Bundaleski, M. Belhaj, T. Gineste, and O. M. N. D. Teodoro, "Calculation of the angular dependence of the total electron yield," Vacuum **122**, 255–259 (2015).
[55]M. J. Sekerak, R. R. Hofer, J. E. Polk, B. a. Jorns, and I. G. Mikellides, "Wear testing of a magnetically shielded Hall thruster at 2000 s specific impulse," in *34th International Electric Propulsion Conference, Kobe, Japan* (2015), pp. IEPC–2015–I155.